Organic Solvent Nanofiltration (OSN) with Spiral-Wound Membrane Elements-Highly Rejected Solute System

Pedro Silva, Ludmila G. Peeva and Andrew G. Livingston*

Department of Chemical Engineering, Imperial College, London SW7 2AZ, United Kingdom
**corresponding author, Tel: +44 (0)20 75945582, Fax: +44 (0)20 75945629,*
E-mail: a.livingston@imperial.ac.uk

Abstract

The performance of organic solvent nanofiltration membranes was studied in a pilot-plant apparatus using a spiral-wound (STARMEM^{TM} 122[1]) membrane element over extended periods, with 0-20 wt % solutions of tetraoctylammonium bromide (TOABr) in toluene. It was found that membrane transport parameters determined from flat sheet membrane tests can be used to accurately predict spiral-wound element performance. A simple model considering uniform pressure/concentration conditions on permeate and retentate sides of the membrane element described experimental flux and rejection trends well for the system studied. The simple model gave similar results to a more complex model that allowed for spatial velocity, concentration and pressure gradients. However, when using a number of elements in series the simple model postulate of uniform conditions will be less accurate, and a complex model which includes spatial gradients, or a simple model that uses an average pressure obtained from experimental pressure drop values, will be required to give accurate predictions.

Key words : Organic solvent nanofiltration; Modelling; Spiral-wound membrane element; Highly-rejected solute.

[1] STARMEM is a trademark of W.R. Grace and Co.

1. Introduction

Membrane separation in non-aqueous solutions, in particular in the nanofiltration range, has great potential for applications in various industries including pharmaceutical, fine chemical synthesis, petrochemical and others [1]. Despite the rapid development of research in this area, most processes are still at laboratory scale, mainly due to the limited choice of solvent stable membranes. It is reported that a large-scale OSN membrane process for solvent recovery in lube-oil dewaxing requires ~20% less energy per unit volume of product than the usual distillation based lube processing. The net annual uplift from the membrane unit is over $ 6 million, thus paying back capital expenditure in less than 1 year [2,3]. This highly successful application at large scale clearly shows the potential for OSN to impact the refining and chemicals sectors. New generations of robust membranes, stable in wide range of organic solvents (including aprotic solvents) are under development [4,5], thus broadening the possibilities for effective industrial applications of OSN.

The development of an industrial membrane process follows a complicated strategy and involves moving from lab-scale coupon-tests, via larger stage-cut experiments and pilot plant tests, to a demonstration plant at the site and ultimately large-scale commercialization. Each step brings an increase in membrane area requirement, equipment, quantity of required feedstocks, time for execution, analytical facilities, technical issues, and operating personnel [6]. Thus the development of an effective mathematical tool for scaling up OSN processes is important for smooth transition between the stages. The most effective way for scaling up the flat sheet membrane area is the spiral-wound element, since it offers a favourable balance between ease of operation, fouling control, permeation rate and packing density [1]. In the OSN research area however, there is still a lack of publications on spiral-wound elements:

- Published work describing spiral-wound nanofiltration refers to aqueous systems [7-11]. There is no literature data, or reports on modelling OSN using spiral-wound elements.
- In order to efficiently implement OSN separation processes based on spiral-wound elements, an engineering design model would be useful.

It is not clear which level of model complexity is required to perform accurate modelling when using spiral-wound element nanofiltration systems. Most of the models presented in the literature for aqueous systems have discrepancies between 5% and 35% when compared with experimental data [12]. However, given the lack of a substantial body of accurate experimental data for OSN, and the early stage of modelling transport processes in these systems, it seems sensible to start with simple models and to advance these, as understanding is improved.

In previous work [13] we have shown that a modified solution-diffusion model for membrane transport, coupled to a film theory approach for the liquid phase mass transfer, was successful for describing highly rejected solute systems under flat-sheet cross-flow conditions. No attempt to test this model application with spiral wound element has yet been reported.

In this study, a pilot plant apparatus was used to determine the flux and rejection behaviour of a spiral-wound STARMEM^{TM} 122 element. The binary system toluene/tetraoctylammonium bromide (TOABr), investigated earlier [13], was specifically chosen to establish comparisons with flat-sheet cross-flow nanofiltration results.

For the spiral-wound element description two models were employed: i) a simple model which considers uniform pressure and concentration on each side of the membrane; and ii) a complex model that takes into account radial and axial variation

of pressure, cross-flow velocity, and concentration. The modified solution-diffusion model was used as a membrane transport model [13] and the film theory was included to describe liquid mass transfer phenomena. The membrane transport parameters obtained from flat-sheet cross-flow experiments [13] were used as input parameters for the latest model.

Through considering the calculated and the experimental results, we seek to gain insight into the usefulness of flat-sheet data for prediction of spiral-wound element performance, and also into what level of model complexity is required to accurately describe OSN using spiral-wound elements.

2. Spiral-wound element modelling

Simple Model

The simplest approach to spiral-wound elements modelling is to consider the element as a flat-sheet membrane and ignore pressure, velocity and concentration gradients throughout the radial and axial dimensions of the element. The concentrations on the permeate and retentate sides of the membrane are assumed to be at the outlet values throughout the element. This simple spiral-wound model reduces to a membrane transport model coupled with the film theory model for solution mass transfer. The detailed mathematical description of the simple spiral-wound model can be found in Table 1 (Eqs. 1-22). The membrane transport is described by Equations 1-8 (detail derivation could be found in [13]), while equation 22 [11] describes the solution mass transfer for a spacer-filled flat channel (see Complex Model section for details). The momentum, velocity and pressure gradients (Eqs. 9,10,11,15,16,17) at the permeate and the retentate side will be zero. Equations 12-14; 18-21 define the boundary conditions.

Complex Model

When a more detailed description of the transport in spiral-wound elements is required, the variation of process variables within the axial and radial dimensions of the element must be taken into account.

Analysis of the published two-dimensional mathematical models for aqueous nanofiltration using spiral-wound elements [7-10] suggests that most systems can be accurately described with a model obeying the following assumptions:

1. Negligible diffusive mass transport in comparison to the convective mass transport along the main flow direction of the spiral-wound channels.
2. Plug flow in both permeate and feed channels.
3. The spiral-wound element is considered to comprise a stack of two flat, spacer-filled channels (curvature of the channels is neglected).

From the above assumptions, and considering the geometry of the system (Fig. 1) the differential solute and solvent material balances can be derived (Eqs. 31,32,37,38 in Table 2). To correctly describe the performance of a spiral-wound element, knowledge about the pressure drop in the feed and permeate channels is essential. Schock and Miquel [11] have shown, that independently of the type of spacers used in a flat channel, for $100 < \mathrm{Re} < 1000$ the pressure drop can be calculated by Eq. 33, and for $\mathrm{Re} < 100$ by Eq. 39. Since in this work we will be dealing with concentrated solutions of highly rejected specie, liquid mass transfer will play an important role in the transport. Previously, it was shown [13, 14] that the film theory model could predict concentration polarization phenomena for OSN of concentrated solutions, once an accurate mass transfer coefficient value is determined. Once again the work of Schock and Miquel [11] provides a correlation able to predict the mass transfer coefficient, for any type of spacer-filled flat channel under common cross-flow

conditions (Eq.44). The membrane transport equations (Eqs. 23-30) are similar to the ones used in the simple model. The set of equations described in the previous paragraph form the complex spiral-wound model and are shown in detail in Table 2 (Eqs. 23-44). A number of membrane element specifications are required as complex spiral-wound model input parameters. These specifications were provided by the element supplier and are described in Table 3. Finally, the membrane transport parameters, obtained from flat-sheet experiments using the same membrane-binary mixture system [13], together with the activity coefficient model determined for Toluene-TOABr mixtures [13], are presented in Table 4.

3. Materials and methods

3.1 Chemicals

Toluene (Tennants Distribution Ltd, UK) was used as a solvent. The quaternary ammonium salt, tetraoctylammonium bromide (98% purity) was purchased from Dishman Pharmaceuticals and Chemicals Ltd. UK.

3.2 Spiral-wound membrane element

The 2.5"x40" STARMEM^{TM} 122 spiral-wound element was manufactured by WR Grace & Co, USA, and was supplied by Membrane Extraction Technology Ltd (UK).

3.3 Experimental procedure

Experiments using the spiral-wound element were performed for several concentrated solutions of TOABr in toluene (0-20%w/w) in order to test the effect of concentration on OSN fluxes and rejections. The experiments were conducted at 30 ^{o}C and three different pressures were tested (10, 20 and 30 bar). The influence of feed flow rate on flux and rejection was also tested for the above pressures.

Fig. 1 shows the diagram of the pilot plant nanofiltration rig. It consists of a spiral-wound nanofiltration element, a feed reservoir, a diaphragm pump, permeate and retentate flow indicators and retentate pressure indicators. The solution enters the spiral wound element at a controlled flow rate and both permeate and retentate are re-circulated to the feed reservoir. The membrane element is held within a pressure housing; this is effectively a flanged stainless steel pipe spool of 2.5" i.d. and overall length 1.15 m, with 1" side entries to the spool (close to the end on the top and bottom at opposite ends of the pipe, see Figure 1A). The key process loop consists of feed tank, pump and the membrane housing. The feed tank (capacity 75 L) is filled using an air-operated diaphragm pump (not shown). A sight glass is present on the side of the feed tank for manual level inspection. The liquid flowrate through this filtration loop can be set on the control panel up to a maximum flow of 1200 $L.h^{-1}$. Any material that passes through the membrane is collected in the permeate line, while any material retained by the membrane flows out of the module through the retentate line. The pressure applied to the membrane is controlled by a back-pressure control valve (PCV); the percentage value that this valve is opened determines the pressure across the membrane. Pressure transducers PIT, PITC measure the transmembrane, retentate and feed pressures respectively. The feed tank has a temperature controller (TTC) with a solenoid valve connected to either a hot water or cooling water line. If the temperature in the feed tank increases above/below the setpoint, RCV2 is driven open by compressed air from RCV1 and allows flow of cooling/heating water through the heat exchanger (HEX). The applied pressure, the temperature and the feed flow rate are controlled by a programmable logic controller.

During filtration the solvent flux was obtained as:

$$N_v = \frac{F}{A} \tag{45}$$

Where F is the permeate volumetric flow rate read on the digital flowmeter and A the effective membrane area. The coefficient of variation for flux at the different pressures was lower than 3.5% for four independent measurements. The observed rejection was defined as

$$OR_i = \left(1 - \frac{C_{ip}}{C_{if}}\right) \times 100\% \quad (46)$$

Where C_{ip} and C_{if} are the concentrations of specie i in the permeate and in the feed respectively.

3.4 Analytical Methods

The concentrations of TOABr were determined using a Perkin-Elmer Gas Chromatograph with a flame ionisation detector and an HP1 methyl siloxane column 30 m long x 0.35mm i.d. The temperature programme ran from 80 ºC to 300 ºC at a rate of 25 ºC.min^{-1}, and the column temperature was held at 80 ºC and 300 ºC for 3 minutes at the start and finish of the temperature programme respectively. The coefficient of variation was 2% for three independent measurements.

4. Results and discussion

Before detailed discussion of the modelling results we should point out the following:

- Both levels of modelling complexity were used in order to describe the experimental results and access the complexity level required for accurate predictions.
- All membrane/liquid mass transfer model input parameters were obtained from [13]. These include solvent/solute permeabilities, solute diffusion

coefficient, solution viscosity/density and solution activity coefficients (Table 4).

- The complex spiral-wound model mathematical description forms a system of partial differential algebraic equations (PDAEs) which was solved by gPROMS using a centred finite difference scheme. The simple spiral-wound model mathematical description consists of a nonlinear system of equations; this was solved using a Newton-Raphson routine implemented by gPROMS.

Flux/Rejection Calculations

The experimental and calculated (from both models) results for the flux and rejection are presented in Figures 2 and 3. Both models describe the experimental flux trends reasonably well. We point out here that the toluene permeability obtained with the spiral-wound element appears to be slightly higher than the one determined from the cross-flow filtration unit (~1.15 vs. 1.10 $mol.m^{-2}.s^{-1}$). Such variations are not uncommon with polymeric membranes; however for the calculations the value obtained with the cross-flow filtration unit was used in order to check the applicability of the cross-flow data for up-scaling purposes, consistent with the aim of this work. That is why both models slightly underestimate the flux, with the complex model giving the lowest values. The mean absolute percentage error given by the complex model is 28%, 9% and 5% at 10, 20 and 30 bar respectively vs. 15%, 5% and 2% for the simple model. This is expected since the simple spiral-wound model assumes constant (maximum) pressure along the whole element length, leading to higher flux predictions than in the complex model, in which pressure decreases in the axial direction. As it will be shown later the complex model slightly overestimates pressure-drop in the feed channel, thus introducing higher discrepancy with the experimental data. For rejection, both models predict exactly the same trend, Fig. 3.

This was expected, since TOABr permeability is very low and rejection throughout is close to 100%.

Stage Cut and Solution Concentration

The stage cut is defined as

$$\frac{\textit{Permeate Flow Rate}}{\textit{Feed Flow Rate}} \times 100\%$$

Stage cuts in the experiments conducted ranged from 1.7 % to 20 %. Importantly, the concentration of TOABr increases axially along the element, leading to a more viscous solution and to a decreasing mass transfer coefficient in the axial direction.

Mass Transfer

As expected, a flux decrease with increasing concentration was observed (Fig. 2). This is common behaviour encountered in the OSN literature and can be explained by the increase in osmotic pressure [13,15], combined with increasing concentration polarization phenomena in more viscous, concentrated solutions [13, 14].

Mass transfer limitations are significant at concentrations above 10 wt % TOABr (Fig. 4). This differs from the results obtained at the cross-flow experiments, where concentration polarisation effects were observed at concentrations as low as ~3 wt %. Equipment limitations restricted flow rates in the system to above 200 $L.h^{-1}$, resulting in calculated mass-transfer coefficients $>3 \times 10^{-5}$ ms^{-1}, while the highest mass-transfer coefficient estimated at the cross-flow unit was $\sim 1.1 \times 10^{-5}$ ms^{-1}, and this difference in effect of concentration can be attributed to the difference between the mass transfer coefficients in the systems. The calculated (complex model) feed channel mass transfer coefficient variation along the spiral-wound element length, for a 225 $L.h^{-1}$ flow rate, is presented in Fig. 5. A linear decrease is predicted, however, this change

is relatively small, and does not significantly affect flux or rejection. Therefore, the simple spiral-wound model assumption of a constant mass transfer coefficient is a good approximation, for systems with sufficiently high feed flow rates.

Pressure Drop

Pressure drop through the element is a crucial factor determining the model complexity required to simulate OSN in spiral-wound elements. The measured feed channel pressure drop values are below the calculated ones, and relatively insignificant (Fig. 6) in particular for the high pressure/high permeating flux systems. In fact the actual pressure drop values should be even lower than the measured ones since we are unable to eliminate the inlet and outlet pressure losses using single spiral wound element [11]. The similarity between the complex and the simple model calculated flux values is also an indication that the feed channel pressure drop is not significant (see Fig. 2). The complex model slightly overestimates pressure drop along the feed channel, however as can be seen from Fig. 6 the discrepancy is below 1 bar. Fig. 6 not only confirms the low pressure drop values in this system but also shows a good agreement between experimental and model calculated feed channel pressure drops, suggesting the applicability of Schock and Miquel's [11] pressure drop correlation to this system. This simplified approach is a good first approximation for system design but as it is based on the assumption of plug flow in both permeate and feed channels it does not provide detailed information about the actual velocity, concentration and pressure profiles at each point of the spacer filled channels of the spiral wound element. That is why for system optimisation purposes, for example optimisation of the channel spacers, application of computational fluid dynamics (CFD) would be more appropriate [16, 17, 18].

According to the complex model predictions, the permeate channel pressure drop is negligible, as it is always bellow 0.02 bar. Therefore, permeate channel pressure drop should not be a significant factor in determining transport through the OSN spiral-wound element system presented in this study.

Although in the system tested the pressure drop values are negligible, we can observe in Fig. 7 an approximately linear relationship between the feed channel pressure drop and the number of spiral-wound elements linked in series. Therefore, in industrial applications where large membrane areas are required, pressure drop might become a really important issue. For instance, for five spiral-wound elements arranged in series, the feed channel pressure drop has a value of approximately 10 bar. Such a high pressure drop value would lead to a considerable flux reduction, and in this case the simple spiral-wound model constant pressure assumption would result in serious miscalculations. Only the complex spiral-wound model would be able to give reasonable flux predictions for such a system, as can be seen in Fig. 8 (1 and 2). However the simple spiral-wound model still can be applied with reasonable accuracy, assuming that the feed channel pressure drop in the system is known, and the arithmetic average trans membrane pressure difference (25 bar in this case) instead of the feed side pressure value (30 bar) is utilized. As can be seen in Fig. 8 (3), when using this approach the complex spiral-wound model values and the simple spiral-wound model calculated flux values differ by less than 15%. It is not possible to develop a "golden rule" for the applicability of the simple model since it strongly depends on the experimental conditions and system properties (e.g. applied pressure, operating temperature, feed flow rate, solvent flux, solution viscosity), in any case the authors will recommend some caution when applying the simple model to a system containing more than one membrane element.

5. Conclusion

Comparison between the experimental and calculated results suggest that the membrane transport parameters obtained from cross-flow experiments using flat sheet membranes could be used for reasonably good estimation of flux and rejection in a OSN spiral-wound element. Thus we speculate that the mathematical models developed on the basis of cross-flow flat-sheet membrane experimental data can provide an useful design tool for OSN processes up-scaling.

Both the complex (Table 1) and the simple spiral-wound models (Table 2) gave a reasonable description of the experimental results. The simple spiral-wound model predictions worked quite well for the system under study, where assumptions of both pressure and mass transfer coefficient constancy were acceptable. However the pressure drop predictions indicate that such a simple model would not be accurate enough for systems with a number of spiral wound elements in series, due to the significantly higher axial pressure drop values generated. In such systems the use of the complex model will be more appropriate.

Acknowledgements

The authors wish to acknowledge the support of Fundação para a Ciência e a Tecnologia Grant Number SFRH/BD/10593/ 2002 for the work described in this paper.

List of Tables

Table 1: Simple spiral-wound model mathematical description.

Membrane Transport Model*

$$N_1 = P_{1m}\left(\frac{c_{1f(m)}}{c_{1f(m)}+c_{2f(m)}} - \frac{c_{1p(m)}}{c_{1p(m)}+c_{2p(m)}}\frac{\gamma_{1p(m)}}{\gamma_{1f(m)}}\exp\left(-\frac{\overline{V}_1\Delta p}{RT}\right)\right) \quad (1)$$

$$N_2 = P_{2m}\left(\frac{c_{2f(m)}}{c_{1f(m)}+c_{2f(m)}} - \frac{c_{2p(m)}}{c_{1p(m)}+c_{2p(m)}}\frac{\gamma_{2p(m)}}{\gamma_{2f(m)}}\exp\left(-\frac{\overline{V}_2\Delta p}{RT}\right)\right) \quad (2)$$

$$c_{1f(m)} = \left(c_{1f} - c_{1p(m)}\right)\exp\left(\frac{N_v}{k}\right) + c_{1p(m)} \quad (3)$$

$$c_{1f(m)}\overline{V}_1 + c_{2f(m)}\overline{V}_2 = 1 \quad (4)$$

$$N_v = N_1\overline{V}_1 + N_2\overline{V}_2 \quad (5)$$

$$c_{1p(m)} = \frac{N_1}{N_V} \quad (6)$$

$$c_{1p(m)}\overline{V}_1 + c_{2p(m)}\overline{V}_2 = 1 \quad (7)$$

$$OR = 1 - \frac{c_{1p}}{c_{1f}} \quad (8)$$

Differential Mass/Momentum Balances

Feed Side		Permeate Side	
$\frac{\partial u_f}{\partial z} = 0$	(9)	$\frac{\partial u_p}{dy} = 0$	(15)
$\frac{\partial (u_f c_{1f})}{\partial z} = 0$	(10)	$\frac{\partial (u_p c_{1p})}{\partial y} = 0$	(16)
$\frac{\partial p_f}{\partial z} = 0$	(11)	$\frac{\partial p_p}{\partial y} = 0$	(17)
$u_f(0,y) = u_{f0}$	(12)	$u_p(z,0) = u_{p0}$	(18)
$c_{1f}(0,y) = c_{1f0}$	(13)	$\frac{\partial c_{1p}(z,0)}{\partial y} = 0$	(19)
$p_f(0,y) = p_{f0}$	(14)	$\frac{\partial p_p(z,0)}{\partial y} = 0$	(20)
		$p_p(z,W) = 0$	(21)

Mass Transfer Coefficient Model

$$\frac{kd_{h_f}}{D_{12}} = 0.065\mathrm{Re}^{0.875}\,Sc^{0.25} \quad (22)$$

*c_{if} and c_{ip} are assumed to be at the outlet values throughout the element and $c_{ip(m)}=c_{ip}$

Table 2: Complex spiral-wound model mathematical description.

Membrane Transport Model

$$\ddot{N}_1 = P_{1m}\left(\frac{\ddot{c}_{1f(m)}}{\ddot{c}_{1f(m)}+\ddot{c}_{2f(m)}} - \frac{\ddot{c}_{1p(m)}}{\ddot{c}_{1p(m)}+\ddot{c}_{2p(m)}}\frac{\gamma_{1p(m)}}{\gamma_{1f(m)}}\exp\left(-\frac{\overline{V}_1\Delta\ddot{p}}{RT}\right)\right) \quad (23)$$

$$\ddot{N}_2 = P_{2m}\left(\frac{\ddot{c}_{2f(m)}}{\ddot{c}_{1f(m)}+\ddot{c}_{2f(m)}} - \frac{\ddot{c}_{2p(m)}}{\ddot{c}_{1p(m)}+\ddot{c}_{2p(m)}}\frac{\gamma_{2p(m)}}{\gamma_{2f(m)}}\exp\left(-\frac{\overline{V}_2\Delta\ddot{p}}{RT}\right)\right) \quad (24)$$

$$\ddot{c}_{1f(m)} = \left(\ddot{c}_{1f} - \ddot{c}_{1p(m)}\right)\exp\left(\frac{\ddot{N}_v}{\ddot{k}}\right) + \ddot{c}_{1p(m)} \quad (25)$$

$$\ddot{c}_{1f(m)}\overline{V}_1 + \ddot{c}_{2f(m)}\overline{V}_2 = 1 \quad (26)$$

$$\ddot{N}_v = \ddot{N}_1\overline{V}_1 + \ddot{N}_2\overline{V}_2 \quad (27)$$

$$\ddot{c}_{1p(m)} = \frac{\ddot{N}_1}{\ddot{N}_V} \quad (28)$$

$$\ddot{c}_{1p(m)}\overline{V}_1 + \ddot{c}_{2p(m)}\overline{V}_2 = 1 \quad (29)$$

$$\ddot{O}R = 1 - \frac{\ddot{c}_{1p}}{\ddot{c}_{1f}} \quad (30)$$

Differential Mass/Momentum Balances

Feed Side

$$\frac{\partial\ddot{u}_f}{\partial z} = \frac{-2\ddot{N}_v}{h_f\varepsilon_f} \quad (31)$$

$$\frac{\partial(\ddot{u}_f\ddot{c}_{1f})}{\partial z} = -2\frac{\ddot{N}_1}{h_f\varepsilon_f} \quad (32)$$

$$\frac{\partial\ddot{p}_f}{\partial z} = \frac{6.23}{2d_{h_f}}\ddot{\mathrm{Re}}^{-0.3}\rho\ddot{u}_f{}^2 \quad (33)$$

$$u_f(0,y) = u_{f0} \quad (34)$$

$$c_{1f}(0,y) = c_{1f0} \quad (35)$$

$$p_f(0,y) = p_{f0} \quad (36)$$

Permeate Side

$$\frac{\partial\ddot{u}_p}{dy} = \frac{2\ddot{N}_v}{h_p\varepsilon_p} \quad (37)$$

$$\frac{\partial(\ddot{u}_p\ddot{c}_{1p})}{\partial y} = 2\frac{\ddot{N}_1}{h_p\varepsilon_p} \quad (38)$$

$$\frac{\partial\ddot{p}_p}{\partial y} = \frac{105}{2d_{h_p}}\ddot{\mathrm{Re}}^{-0.8}\rho\ddot{u}_p{}^2 \quad (39)$$

$$u_p(z,0) = 0 \quad (40)$$

$$\frac{\partial c_{1p}(z,0)}{\partial y} = 0 \quad (41)$$

$$\frac{\partial p_p(z,0)}{\partial y} = 0 \quad (42)$$

$$p_p(z,W) = 0 \quad (43)$$

Mass Transfer Coefficient Model

$$\frac{\ddot{k}d_{h_f}}{D_{12}} = 0.065\ddot{\mathrm{Re}}^{0.875}\ddot{S}c^{0.25} \quad (44)$$

$\ddot{V}ariable$ - Indicates that the model variables are functions of axial (z) and radial (y) coordinates.

Table 3: Spiral-wound element specifications.

W (mm)	L (mm)	h_p (mm)	ε_p (-)	d_{h_p} (mm)	h_f (mm)	ε_f (-)	d_{h_f} (mm)
350	861	0.80	0.40	0.63	0.70	0.73	1.02

Table 4: Flat-sheet membrane model parameter values (obtained from [13]).

Compound	Toluene	TOABr
Diffusion Coefficient ($m^2.s^{-1}$)	-	0.88×10^{-9}
Molar Volume ($m^3.mol^{-1}$)	106×10^{-6}	766×10^{-6}
Membrane Permeability ($mol.m^{-2}.s^{-1}$)	1.10	3×10^{-5}
Activity coefficient (-)	$\gamma_{Toluene} = -4.16x_{Toluene}^2 + 7.29x_{Toluene} - 2.13$	$\gamma_{TOABr} = 1$

List of Figures

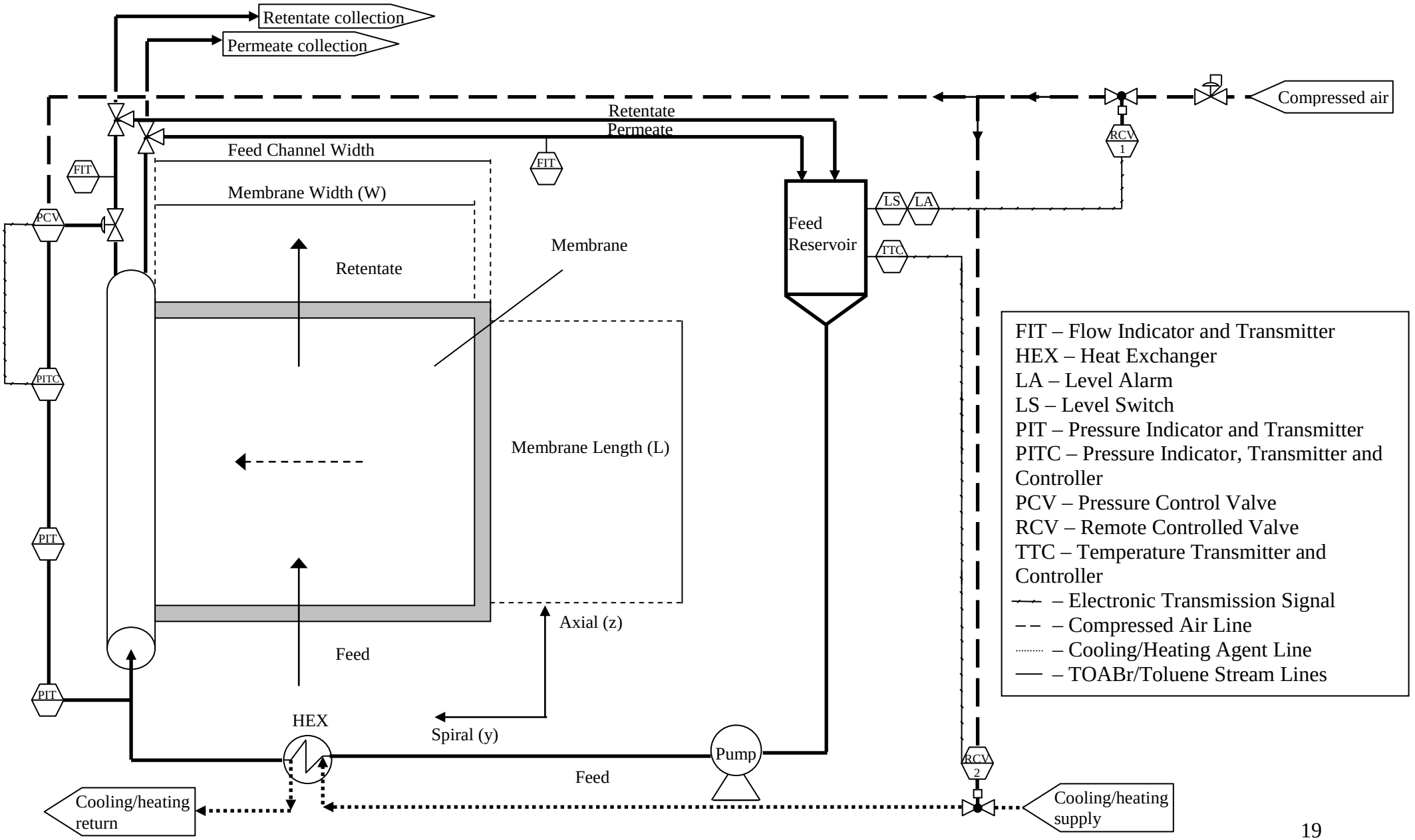

Figure 1: Pilot plant unit with spiral-wound element (element shown schematically as unwound).

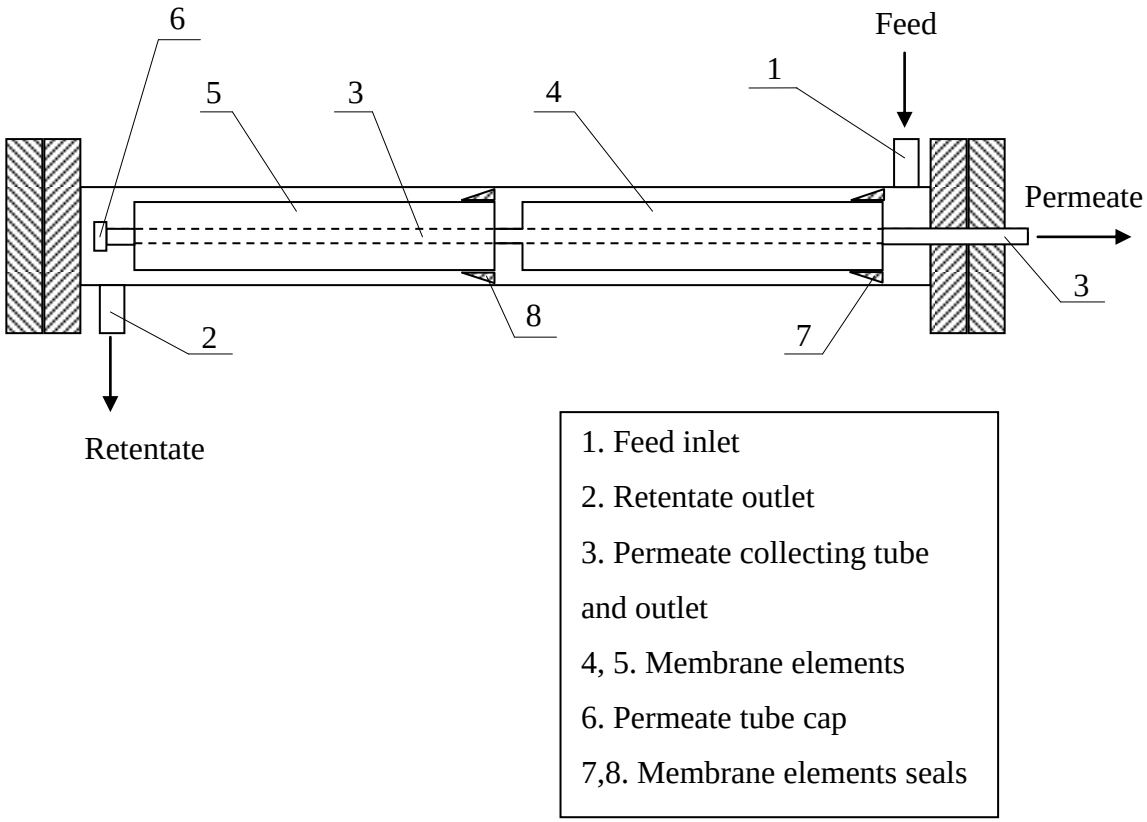

Figure 1A: Schematic representation of membrane element housing, containing two membrane elements in series. Please note that the second element is added only for illustration purposes, all experiments in this study were performed using a single membrane element.

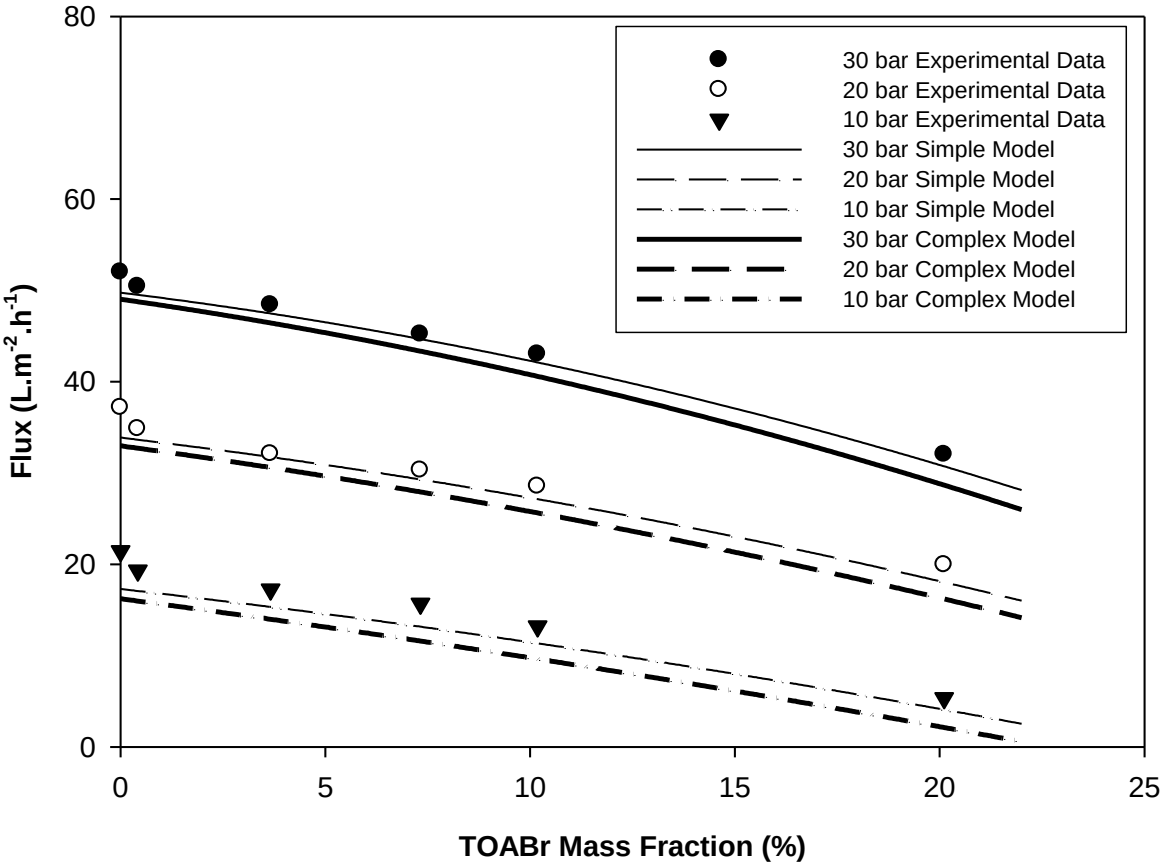

Figure 2: Experimental and calculated flux of toluene/TOABr mixtures at several pressures, 30 ^{o}C and feed flow rate 550 Lh^{-1}.

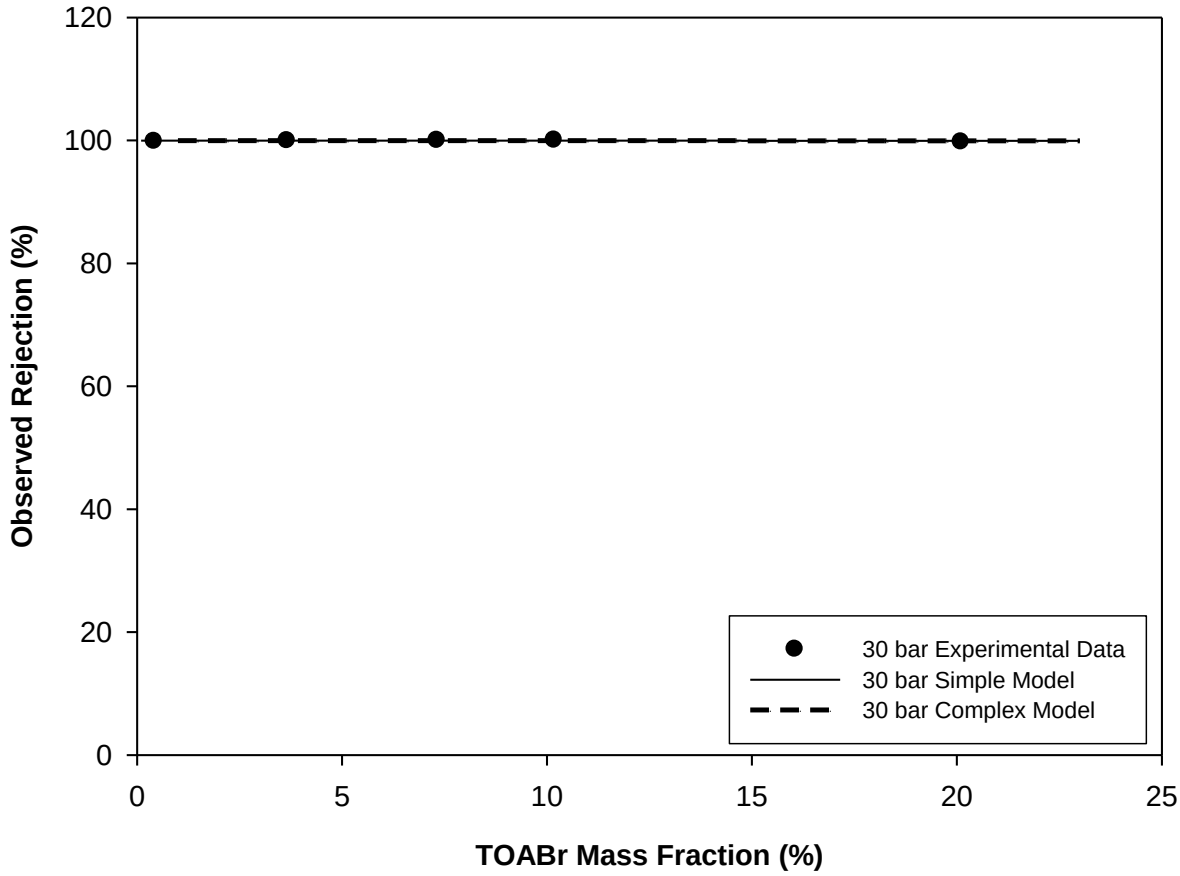

Figure 3: Experimental and calculated TOABr observed rejection for toluene/TOABr mixtures at 30 bar, 30 ^{o}C and feed flow rate 550 Lh^{-1}.

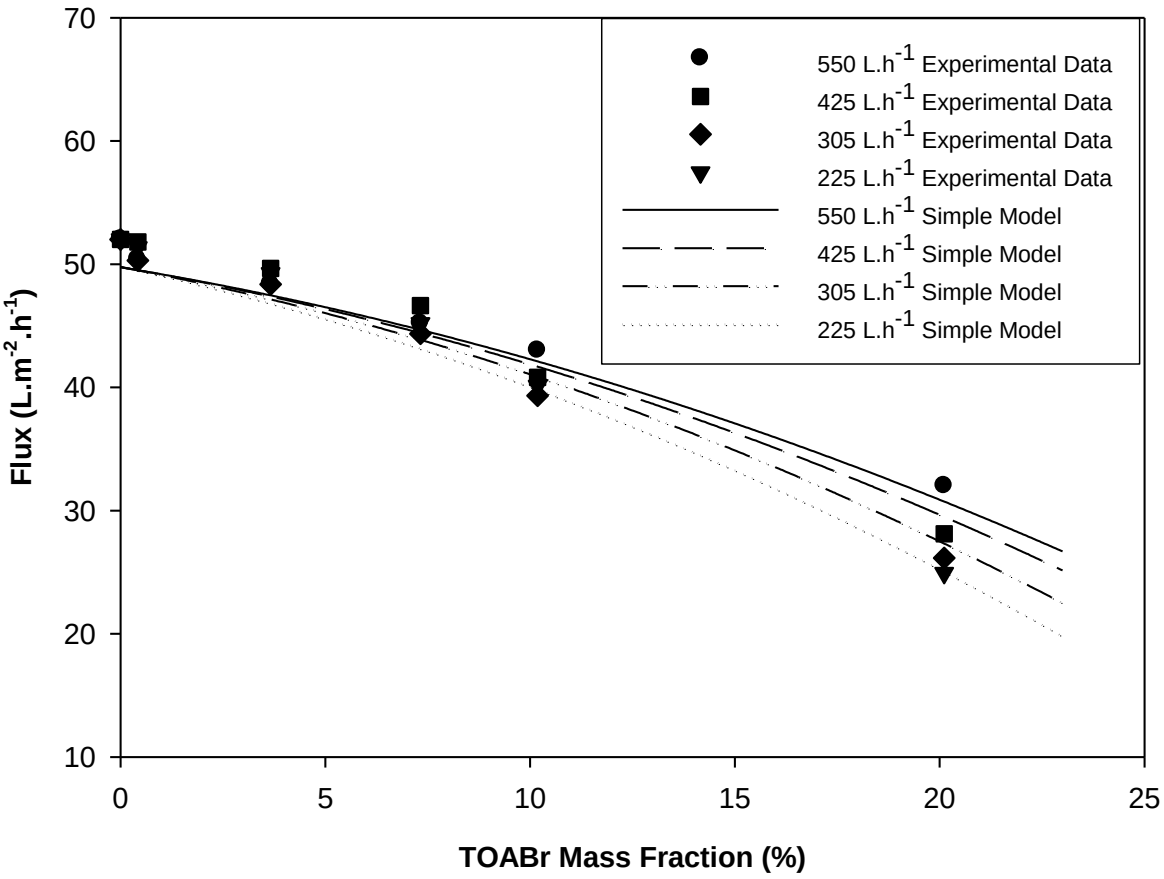

Figure 4: Experimental and calculated flux of toluene/TOABr mixtures for several feed flow rates, at 30 bar and 30 ^{o}C.

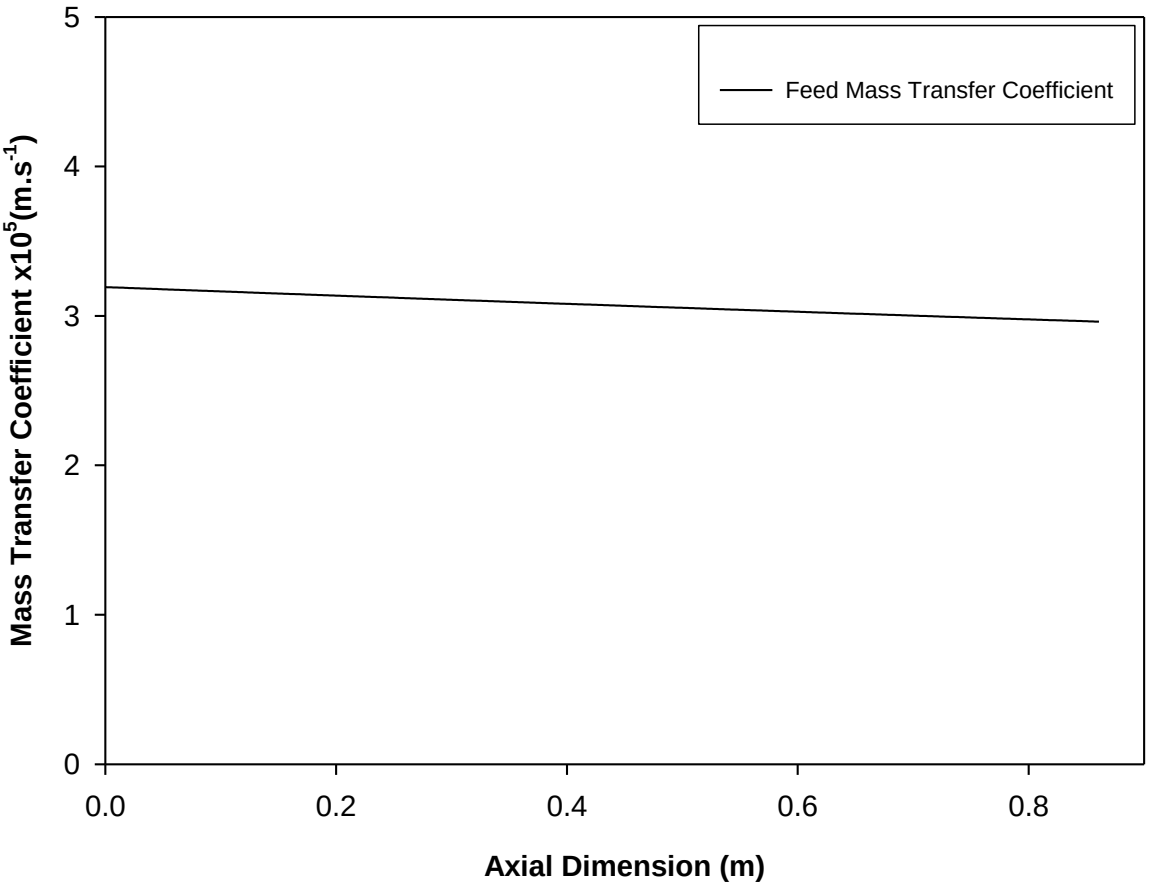

Figure 5: Calculated (complex model) feed channel mass transfer coefficient, at 30 bar, 30 ^{o}C, 225 L.h^{-1} feed flow rate and 20 % TOABr mass fraction as a function of axial distance along the spiral element from feed side.

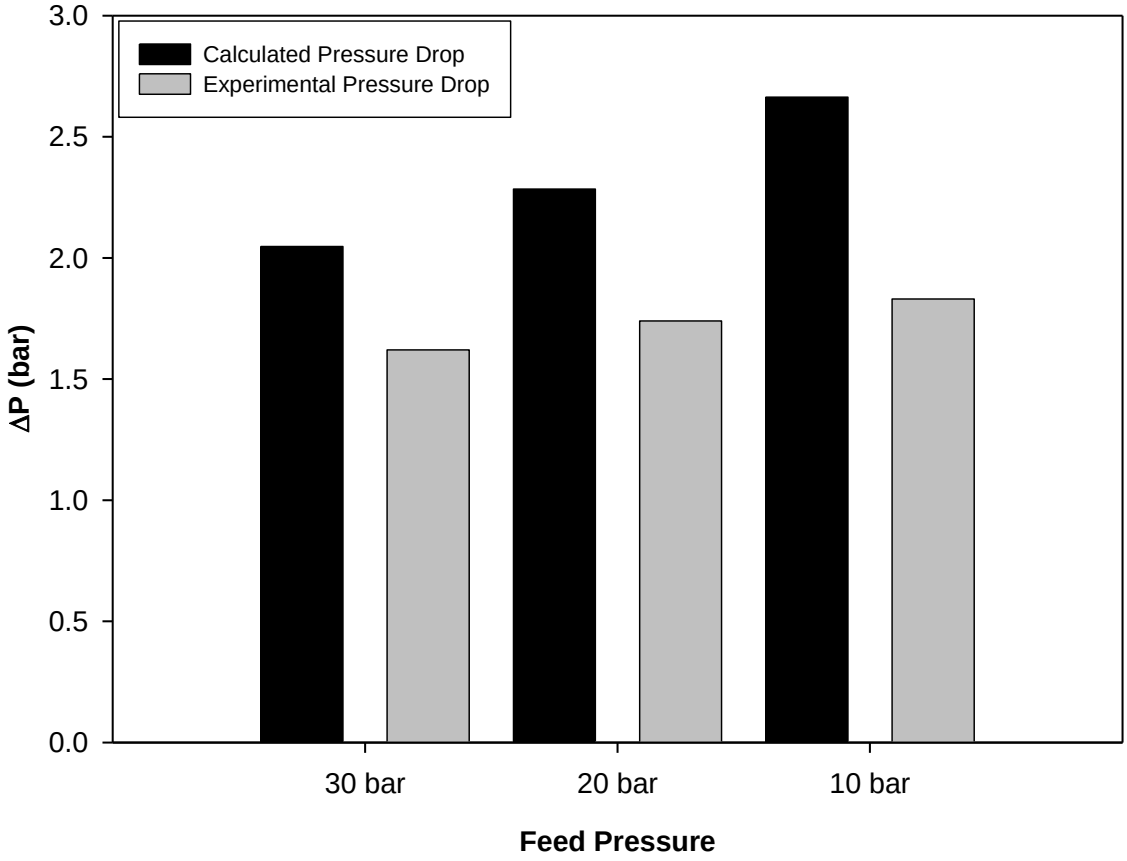

Figure 6: Experimental and calculated (from the complex model) values for the axial pressure drop in the spiral-wound element at 30 ^{o}C, 550 L.h^{-1} feed flow rate and 20 % TOABr mass fraction.

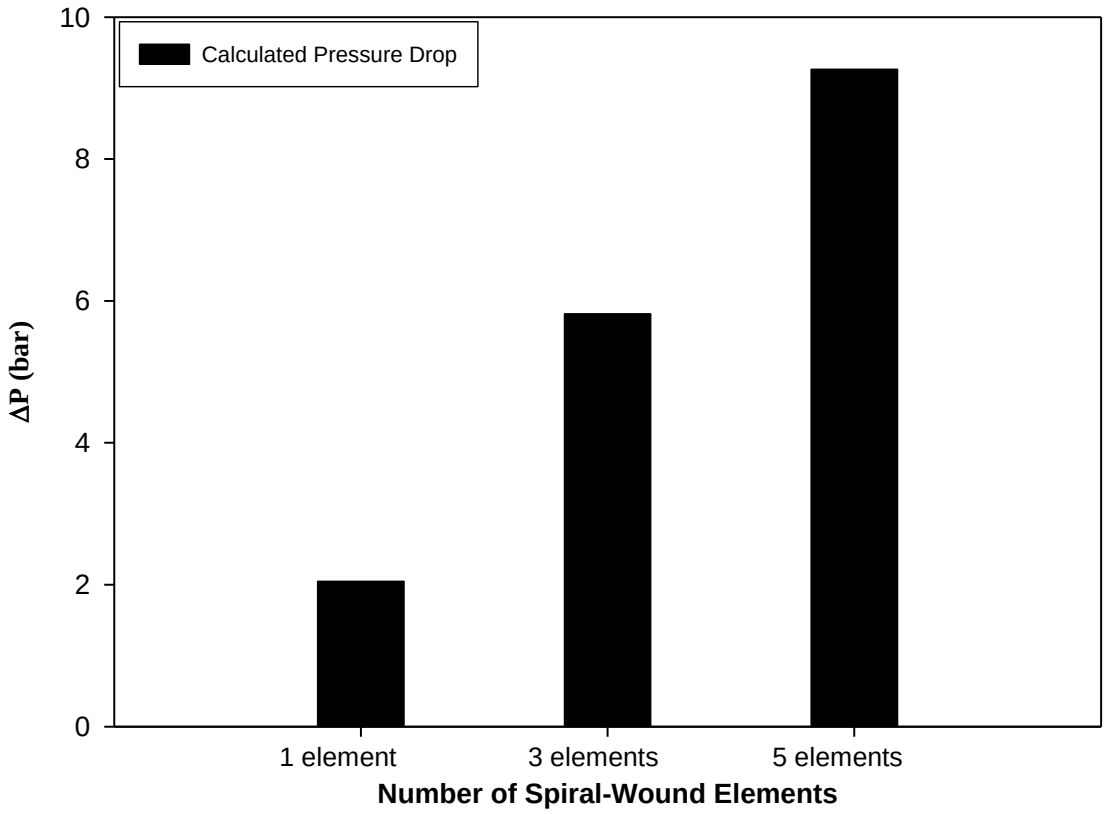

Figure 7: Calculated (from the complex model) pressure drop values at 30 ^{o}C, 30 bar, 550 L.h^{-1} feed flow rate and 20 % TOABr mass fraction for various numbers of membrane elements in series.

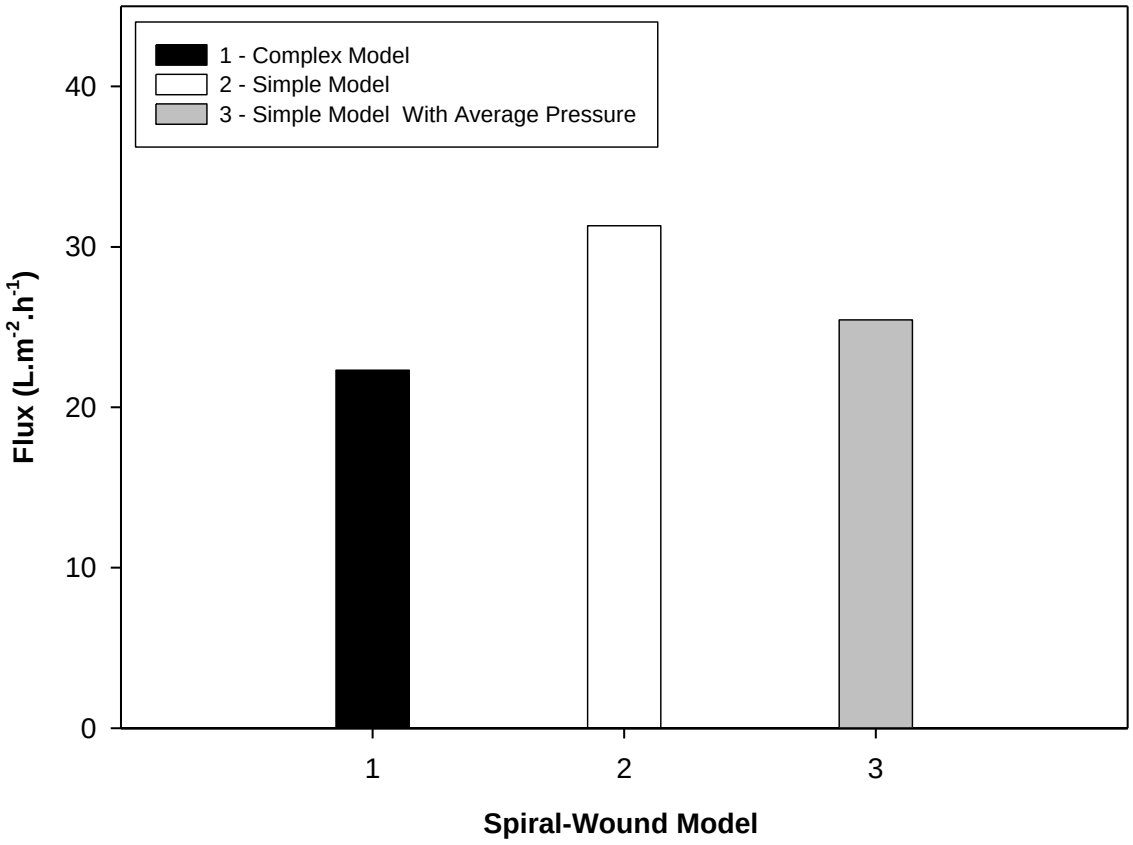

Figure 8: Calculated flux values at 30 ^{o}C, 30 bar, 550 L.h^{-1} feed flow rate and 20 % TOABr mass fraction for a system consisting of 5 membrane elements in series.

Nomenclature

A	Membrane area (m^2)
c	Molar concentration ($mol.m^{-3}$)
d_h	Hydraulic diameter of the channel (m)
D_{12}	Solute diffusion coefficient ($m^2.s^{-1}$)
F	Total volumetric flow rate ($m^3.s^{-1}$)
h	Height of the channel (m)
k	TOABr mass transfer coefficient ($m.s^{-1}$)
L	Length of the spiral-wound element (m)
N	Molar flux ($mol.m^{-2}.s^{-1}$)
N_v	Total volumetric flux ($m.s^{-1}$)
OR	Observed rejection (-)
p	Pressure (Pa)
P	Molar Permeability ($mol.m^{-2}.s^{-1}$)
R	Ideal gas constant ($Pa.m^3.mol^{-1}.K^{-1}$)
Re	Reynolds number (-)
Sc	Schmidt number (-)
T	Temperature (K)
u	Velocity ($m.s^{-1}$)
V	Volume (m^3)
$\overline{V}$	Partial molar volume ($m^3.mol^{-1}$)
W	Width of the spiral-wound element (m)

Greek letters

γ	Molar activity coefficient (-)
ρ	Density ($Kg.m^{-3}$)
ε	Porosity (-)

Subscripts

f	Feed side
i	Species
m	Membrane
(m)	At the membrane-liquid interphase
p	Permeate side

References

[1] P. Vandezande, L.E. M. Gevers, I.F.J. Vankelecom, Solvent resistant nanofiltration: separating on a molecular level, Chem. Soc. Rev. 37 (2008) 365-405.

[2] N.A. Bhore, R.M. Gould, S.M. Jacob, P.O. Staffeld, D. McNally, P.H. Smiley, C.R. Wildemuth, New membrane process debottlenecks solvent dewaxing unit, Oil Gas J. **97** (46) (1999) 67–74.

[3] L. S. White, A. R. Nitsch, Solvent recovery from lube oil filtrates with a polyimide membrane, J. of Membr. Sci., 179 (2000) 267-274.

[4] Y.H. See Toh, F.W. Lim, A.G. Livingston, Polymeric membranes for nanofiltration in polar aprotic solvents, J. Membr. Sci. 301 (2007) 3–10.

[5] I. Voigt, Nanofiltration mit keramischen membranen, Chemie Ingenieur Technik 77 (2005), 559-564.

[6] L. S. White, Development of large-scale applications in organic solvent nanofiltration and pervaporation for chemical and refining processes, J. Membr. Sci. 286 (2006) 26–35.

[7] A. Chiolle, G. Gianotti, M. Gramondo and G. Parrini, Mathematical model of reverse osmosis in parallel-wall channels with turbulence promoting nets , Desalination, 26 (1978) 3-16.

[8] R. Rautenbach and W. Dahm, Design and optimization of spiral-wound and hollow fiber RO-modules, Desalination, 65 (1987) 259-275.

[9] F. Evangelista and G. Jonsson, Optimal design and performance of spiral wound modules. I. Numerical method, Chem. Eng. Comm., 72 (1988) 69-81.

[10] M.B. Boudinar, W.T. Hanbury and S. Avlonitis, Numerical simulation and optimisation of spiral-wound modules, Desalination, 86 (1992) 273-290.

[11] G. Schock and A. Miquel, Mass transfer and pressure loss in spiral wound modules , Desalination, 64 (1987) 339-352.

[12] J. Schwinge, P. R. Neal, D. E. Wiley, D. F. Fletcher, A. G. Fane, Spiral wound modules and spacers-Review and analysis, J. Membr. Sci., 242 (2004) 129-153.

[13] L.G. Peeva, E. Gibbins, S.S. Luthra, L.S. White, R.P. Stateva, A.G. Livingston, Effect of concentration polarisation and osmotic pressure on flux in organic solvent nanofiltration, J. Membr. Sci., 236 (2004) 121-136.

[14] P. Silva, A.G. Livingston, Effect of solute concentration and mass transfer limitations on transport in organic solvent nanofiltration-partially rejected solute, J. Membr. Sci., 280 (2006) 889-898.

[15] N. Stafie, D.F. Stamatialis, M. Wessling, Insight into the transport of hexane-solute systems through tailor-made composite membranes, J. Membr. Sci., 228 (2004) 103-116.

[16] F. Li, W. Meindersma, A.B. de Haan, T. Reith, Optimization of commercial net spacers in spiral wound membrane modules. J. Membr. Sci., 208 (2002) 289–302.

[17] J.L.C. Santos, V. Geraldes, S. Velizarov, J.G. Crespo, Modelling of flow and concentration patterns in spiral wound membrane modules with ladder-type spacers. Desalination, 200 (2006) 395–396.

[18] S. Wardeh, H.P. Morvan, CFD simulations of flow and concentration polarization in spacer-filled channels for application to water desalination. Chem. Eng. Res. Des., 86 (2008) 1107–1116.